Correlation between mechanical behavior and actuator-type performance of Ni-Ti-Pd high-temperature shape memory alloys

Glen S. Bigelow*, Santo A. Padula II*, Anita Garg[#], Ronald D. Noebe*
*NASA Glenn Research Center, 21000 Brookpark Road, Cleveland, OH USA 44135;
[#]University of Toledo/NASA Glenn Research Center, Cleveland, OH USA 44135

ABSTRACT

High-temperature shape memory alloys in the NiTiPd system are being investigated as lower cost alternatives to NiTiPt alloys for use in compact solid-state actuators for the aerospace, automotive, and power generation industries. A range of ternary NiTiPd alloys containing 15 to 46 at.% Pd has been processed and actuator mimicking tests (thermal cycling under load) were used to measure transformation temperatures, work behavior, and dimensional stability. With increasing Pd content, the work output of the material decreased, while the amount of permanent strain resulting from each load-biased thermal cycle increased. Monotonic isothermal tension testing of the high-temperature austenite and low temperature martensite phases was used to partially explain these behaviors, where a mismatch in yield strength between the austenite and martensite phases was observed at high Pd levels. Moreover, to further understand the source of the permanent strain at lower Pd levels, strain recovery tests were conducted to determine the onset of plastic deformation in the martensite phase. Consequently, the work behavior and dimensional stability during thermal cycling under load of the various NiTiPd alloys is discussed in relation to the deformation behavior of the materials as revealed by the strain recovery and monotonic tension tests.

Keywords: High-temperature shape memory alloy, NiTiPd, martensite, austenite, tensile properties, work output, shape memory behavior, transformation strain, critical stress for slip, strain recovery.

1.0 INTRODUCTION

The shape memory effect was first discovered in the Au-Cd system in 1951 [1] and later in the Ni-Ti system in 1961 [2]. Since then, NiTi has become widely used in the medical field and is receiving increased attention in the aerospace, automotive, and power generation industries because of its extraordinary properties, such as superelasticity, high work output, stable microstructure, and corrosion resistance [3, 4]. For example, when transformed under load, NiTi can do work equivalent to 10-20 J/cm^3 [5, 6], and when unconstrained, it is capable of recoverable strains of up to eight percent [7]. However, the maximum working temperature for NiTi is approximately 70°C [8], restricting its use to near room temperature applications.

It has been long known that alloying NiTi with Pd, Pt, Au, Hf, or Zr at greater than 10 at.% ternary addition can be used to increase the transformation temperatures [9-16]. While the amount of research on these ternary high-temperature shape memory alloys (HTSMA's) has increased dramatically in the last decade, the majority of the work performed on these alloys has been limited to determining transformation temperature, tensile properties, and unconstrained shape recovery behavior. Very little effort has been focused on actuator-type behavior, for which constrained tests such as thermal cycling under a constant load are more appropriate indicators of performance. Even more surprising is the lack of understanding in ternary and even binary alloys regarding active deformation mechanisms responsible for recoverable and non-recoverable behaviors. For example, it is widely accepted that recoverable detwinning of martensite during a monotonic tensile test begins at an obvious yield point (the deviation from a linear σ-ε response), but there is little agreement as to exactly where dislocation processes in the martensite begin to occur resulting in non-recoverable strain. The onset of slip has been assumed to occur anywhere from the end of the primary detwinning plateau [17], to the end of the second "elastic" modulus curve and the beginning of the secondary plateau [18, 19]. In this investigation, we have used uniaxial tensile tests and unconstrained shape memory recovery data to try to understand the load-biased thermal cyclic response of a series of high-temperature shape memory alloys based on the NiTiPd system. The goal is to begin to understand the recoverable and non-recoverable components of deformation during test conditions similar to those encountered during use in actuator type applications, and thus develop improved alloys.

2.0 MATERIALS AND PROCEDURES

2.1 Material processing and characterization

Five alloys with titanium-rich target compositions $Ni_{49.5-X}Ti_{50.5}Pd_X$ (X = 15, 20, 25, 30, and 46 at.%) were vacuum induction melted in graphite crucibles under a protective argon atmosphere using high purity elemental constituents (99.98 wt.% Ni, 99.995 Pd, 99.95 Ti) and cast into a 25.4 mm diameter by 102 mm long copper mold with a conical hot top section to accommodate shrinkage within the casting. The resulting ingots were vacuum homogenized for 72 hours at 1050°C and furnace cooled. After homogenization, the ingots were sealed in mild steel cans and extruded at 900°C at an area reduction of 7:1.

Each extrusion was sectioned into 50.8 mm long cylindrical blanks using a wire electrical discharge machine (EDM). Blanks were center drilled on each end and rough turned on a computer numerically controlled (CNC) lathe. Final machining of the samples on the CNC lathe produced cylindrical dog-bone shaped tensile samples with 3.81 mm diameter by 16.4 mm long gage sections and threaded button ends. To relieve any possible residual stresses from the machining operation, all of the samples were annealed at 400°C for one hour and furnace cooled. At this point, the samples were considered as being in the as-extruded or "virgin" state.

Chemical compositions of each alloy were quantitatively measured while in this stress relieved state. Metallic elements were measured using inductively coupled plasma emission spectroscopy, while LECO N/O and C/S determinators were used to measure nitrogen, oxygen, carbon, and sulfur contents. Each alloy was mounted, polished, and imaged in a JEOL 840 SEM and Hitachi 4700 FE-SEM to determine the basic microstructure of the alloys and the relative volume fractions and compositions of any minority phases and particles. All phases in the $Ni_{19.5}Pd_{30}Ti_{50.5}$ alloy were positively identified using TEM and EDS analysis. This information was then utilized to identify and quantify the phases present in the remaining four alloys.

2.2 Mechanical testing

All mechanical testing was performed on an MTS 810 servo-hydraulic load frame managed with an MTS FlexTest SE digital controller allowing operation and triggering of multiple control channels simultaneously. Samples were held by threaded inserts, which were screwed into hot grip extension rods held by water cooled hydraulic collet grips. Load was measured with a 100 kN/22 kip load cell. Strain within the gage section was measured with a high-temperature water-cooled extensometer having a 12.7 mm gage length and -10/+20% strain range using alumina extension rods with v-chisel tips held in contact with the sample surface by a frictionless knife edge holding fixture. A GC Controls temperature controller with remote setpoint was coupled with an Ameritherm Novastar 7.5 kW induction heater to heat the samples, while cooling was aided by a muffin fan attached to one side of the load frame. One type K thermocouple was spot welded to each threaded insert and monitored temperature at the sample extents. Temperature at the middle of the gage section was measured by a type K thermocouple spot welded in series to thin 0.127 mm diameter type K thermocouple wire. This thin wire was then spot welded directly to the sample surface using a very low power setting to minimize surface damage from the welding process.

Load-bias tests were conducted in tension by straining the sample at a rate of $1x10^{-4}sec^{-1}$ until the desired stress was reached. While at constant stress, the sample was thermally cycled twice from the martensitic state through the transformation to the austenitic state, and back again. Samples were stressed in successive steps to 0, 99, 197, 295, 393, and 517 MPa, or until failure occurred. Transformation temperatures (A_s, A_f, M_s, and M_f) were measured from the second thermal cycle at each stress level using the intersection of fit lines through the transformation and the linear coefficient of thermal expansion (CTE) regions of the curves (Figure 1). Transformation strain was measured as the difference between the strains at the austenite finish and austenite start intersections. Work output at each stress level was calculated by multiplying the transformation strain by the applied stress. Permanent deformation was measured as the strain difference between the beginning of the heating curve and the end of the cooling curve. All of these measured values are clearly defined in Figure 1.

Monotonic isothermal tension tests were performed on as-extruded, or "virgin" specimens at temperatures 50°C below the martensite finish (M_f) and 50°C above the austenite finish temperature (A_f) to ensure the samples were in the martensite and austenite conditions during testing. Samples were heated in stress control at 0 MPa, to prevent load buildup from thermal expansion, and allowed to soak at temperature for approximately five minutes. After this period,

the samples were strained to failure at a rate of $1x10^{-4}sec^{-1}$. While there was a definite linear elastic portion to the austenitic stress-strain curves, the elastic portion of the martensitic curves was nonlinear, making it difficult to measure the onset of yielding. Consequently, yield for all tests was determined by the 0.2% offset yield stress method.

The "step test" discussed in this paper is a modification of the well known strain recovery test used for shape memory alloys. Here, a sample was loaded in the martensite state at a temperature of $M_f-50°C$ in increasing increments of 0.1% strain, between which, the sample was unloaded, heated to approximately 100°C above the austenite finish ($A_f+100°C$), cooled below the original test temperature and then reheated to the test temperature where the next loading step began (Figure 2). Loading and unloading were performed at a strain rate of $1x10^{-4}sec^{-1}$. The maximum stress and maximum applied strain were measured at the end of each loading step, just prior to unloading (Figure 2). Residual strain from each load/unload step was measured at the end of the unloading curve (Figure 2), and permanent strain was measured as the strain remaining after the thermal cycle was completed and just prior to reloading (Figure 2). The critical stress for dislocation slip in the martensite was estimated by taking the 0.02% offset "yield stress" of the curve formed by plotting the maximum stress for each cycle versus the permanent strain at the end of that cycle. The fraction of the residual strain recovered as a function of the maximum applied strain was also determined using Equation 1.

$$f_{re\,cov\,ered}^{residual} = \frac{\varepsilon_{residual} - \varepsilon_{permanent}}{\varepsilon_{residual}}$$ (1)

3.0 RESULTS

3.1 Material characterization

The measured compositions, within the error of the analytical technique, were consistent with the original aim compositions. Nickel was on target with a maximum measured deviation of ±0.08 at.%, Pd deviated by a maximum of 0.2 at.% Pd above target, and titanium compositions averaged 49.6±0.3 at.%. Quantitative chemical analysis revealed that the impurity contents of the alloys were 0.4±0.1 at.% C, 0.014±0.009 at.% N, and 0.25±0.15 at.% O, with the carbon coming from the graphite crucible used for melting.

Chemical analysis of the extruded and heat treated alloys indicated that all the alloys were essentially stoichiometric, with measured Ti:(Ni+Pd) ratios ranging from 49.9:49.6 to 49.4:49.7. However, microstructural analysis indicated that the alloys were slightly Ti-rich, consistent with their target composition. Scanning electron microscopy revealed a predominantly single phase martensitic matrix with a low density distribution of two types of second phase particles in all five alloys. A representative micrograph for the $Ni_{19.5}Ti_{50.5}Pd_{30}$ alloy is shown in Figure 3. In order to identify different phases, a detailed microstructural analysis was conducted on the $Ni_{19.5}Ti_{50.5}Pd_{30}$ alloy using SEM, TEM and XRD techniques. These analyses revealed a B19 orthorhombic martensite, as expected for ternary NiTiPd alloys containing more than 10 at.% Pd [20,21]. The second phase particles consisted of a Ti-rich phase containing predominantly carbon, but also some oxygen, and an intermetallic phase containing Ti, Ni, and Pd. Electron diffraction and EDS analysis of the former phase indicated that it was an fcc-structured Ti(C,O), while the intermetallic phase was a $Ti_2(Ni,Pd)$ phase isostructural with the face-centered-cubic Ti_2Ni phase found in binary titanium-rich NiTi alloys [22]. It should be mentioned that the presence of O has been shown to stabilize a $Ti_4Ni_2O_x$ phase in NiTi alloys [23, 24]. This phase has the same lattice parameter and the crystal structure as the Ti_2Ni phase since O resides interstitially in the $Ti_4Ni_2O_x$ phase, which also makes it hard to detect. Thus, it is likely that the $Ti_2(Ni,Pd)$ phase in our alloys is also an O-stabilized $Ti_4(Ni,Pd)_2O_x$ phase. The blocky morphology of this phase suggests that it formed interdendritically during solidification and then broke up during extrusion.

Room temperature analysis of the other four alloys (Pd = 15, 20, 25, 46 at.%) by SEM and EDS revealed that they too were made up of a martensitic matrix interspersed with a small volume fraction of Ti(C,O) and $Ti_2(Ni,Pd)/Ti_4(Ni,Pd)_2O_x$. In all five alloys, the average particle sizes of the two phases were ~1.1 and 1.5 μm for the Ti(C,O) and $Ti_2(Ni,Pd)/Ti_4(Ni,Pd)_2O_x$ respectively, with the total particle volume fraction being less than 4%.

Transformation temperatures of the alloys were determined via unconstrained thermal cycling as described in the previous section. The samples were thermally cycled under zero load from 50°C to at least 100°C above where the transformation was seen to finish and then cooled back to 50°C (Figure 4). These temperatures as well as the hysteresis measurements (A_f-M_s) are shown in Table 1. There is a linear increase in all transformation temperatures with increasing Pd content, but the hysteresis remains constant at ~10°C for all alloys except $Ni_{3.5}Ti_{50.5}Pd_{46}$ where it grows to 28°C.

Table 1: Unconstrained transformation temperatures and hysteresis

Composition (at.%)			Extrusion	Transformation Temperature (°C)				Hysteresis (°C)
Ni	Ti	Pd		M_F	M_S	A_S	A_F	A_F-M_S
34.5	50.5	15	36	65	73	75	83	10
29.5	50.5	20	37	123	132	133	143	11
24.5	50.5	25	38	178	190	193	197	7
19.5	50.5	30	24	233	249	250	259	10
3.5	50.5	46	50	469	485	509	513	28

3.2 Constant-load strain-temperature behavior

Our primary interest in high-temperature shape memory alloys is in their potential to be used as solid state actuators and as major components in adaptive structures, primarily for aeronautic applications. Consequently, constant-load strain-temperature (load-biased) tests were performed on each of the alloys as a method for evaluating the work output and dimensional stability under various constant loads. In the embodiment presented here, a single sample was used to effectively screen an alloy to determine its potential as an actuator material by loading it to increasing stress levels (in our case 0, 99, 197, 295, 393, and 517 MPa or until failure occurs), and thermally cycling the alloy twice through the transformation regime at each stress level to determine the transformation strain, work output, and permanent deformation.

Figure 5 depicts the second thermal cycle at each stress level for a standard load-biased test performed on the $Ni_{19.5}Ti_{50.5}Pd_{30}$ alloy. Above each curve, the applied stress and resulting work output are shown. While the load-biased strain-temperature curves for the other alloys are not shown due to space limitations, the transformation strain, work output, and permanent deformation strain for each alloy were compiled and are shown in Figures 6, 7, and 8, respectively. None of these plots report data from the $Ni_{3.5}Ti_{50.5}Pd_{46}$ alloy since the alloy produced no work output even at 99 MPa, but instead, when cycled through the transformation to the austenite state, simply elongated to failure.

In general, the transformation strain increased with increasing stress up to a certain point (197 MPa for the alloy with 15 at.% Pd, and 295 MPa for the alloys with 25 and 30 at.% Pd) (Fig. 6). At stresses below this maximum, the transformation strain increased with stress, because the higher stresses were able to cause more of the martensite twins to reorient in an orientation that favored the applied strain during cooling, and therefore there was more strain available to be recovered during the transition to austenite. At higher stress levels, this reorientation effect is maximized, but the stresses (internal and external) become high enough to prevent full recovery of all the reoriented martensite [25, 26, 27], and so the transformation strain level begins to decrease. Work output, being the mathematical product of the transformation strain and the applied stress, increased with applied stress for all of the stress levels reached, but would be expected to decrease at higher stress levels if they were attained, as our previous work in compression has shown [28].

The permanent deformation that occurred during each cycle (Figure 8) increased with both increasing Pd content and increasing stress level. However, some permanent deformation was observed at every stress level tested, indicating poor dimensional stability of the NiTiPd alloys regardless of Pd content. This result was somewhat unexpected given the low temperatures and stresses that were involved in testing, for example in the case of the $Ni_{34.5}Ti_{50.5}Pd_{15}$ alloy, and given previous results for other HTSMA's such as $Ni_{30}Ti_{50}Pt_{20}$ [29]. Consequently, additional testing was performed to gain insight into possible causes of this plastic deformation and the behavior of this group of alloys in general.
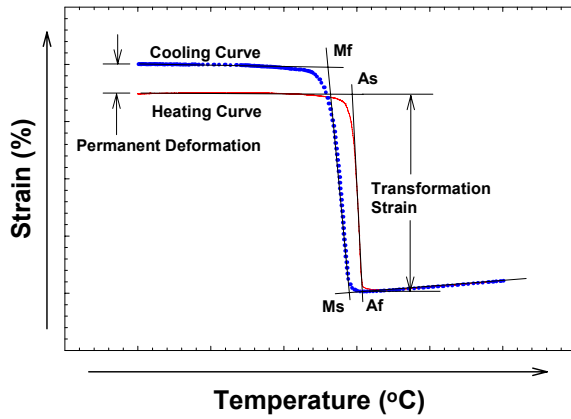
Figure 1: Schematic of a load-biased strain temperature cycle with measured values defined.
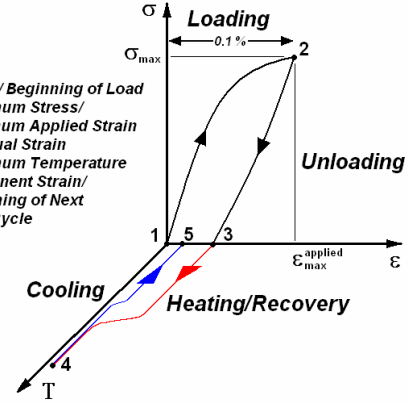

Figure 2: Schematic of an unconstrained strain recovery step test showing measurement points 1-5. Undercooling and reheating are omitted for clarity.
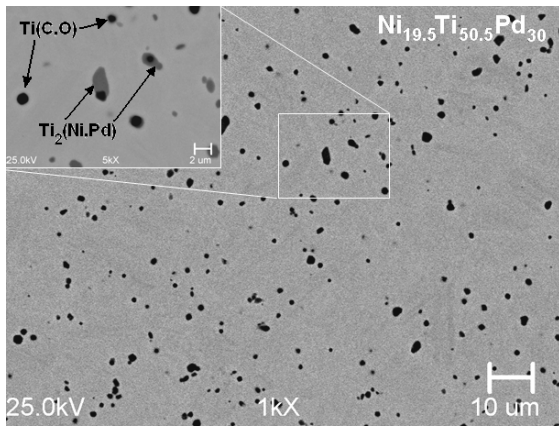

Figure 3: Room temperature backscattered electron image of the microstructure of the $Ni_{19.5}Ti_{50.5}Pd_{30}$ alloy showing secondary phases in a B19 martensite matrix.
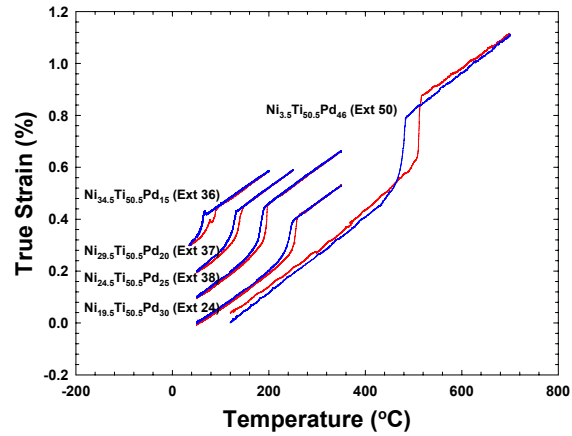

Figure 4: No-load transformation curves for all five alloys showing increasing transformation temperatures with increasing Pd content.
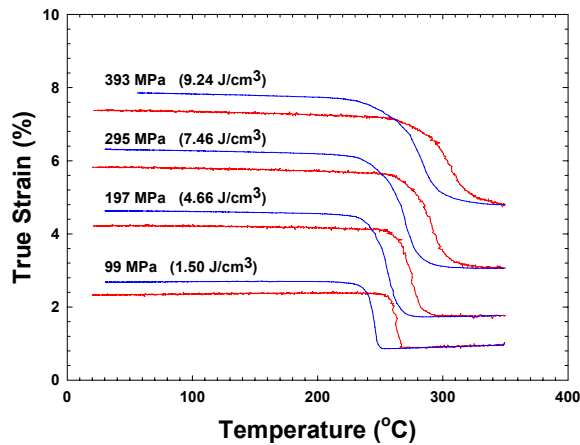
Figure 5: Load-biased strain-temperature curves for the $Ni_{19.5}Ti_{50.5}Pd_{30}$ alloy showing the second cycle at each stress level.
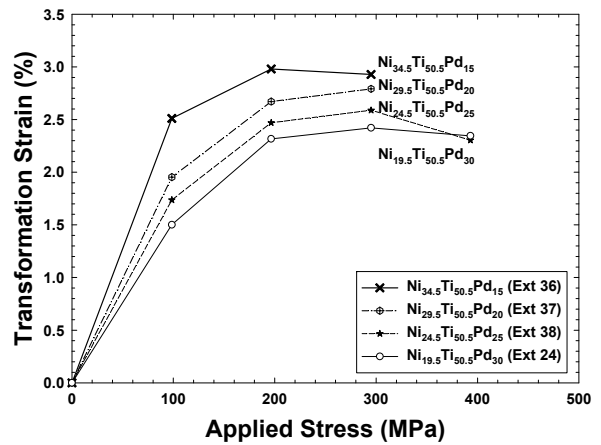

Figure 6: Transformation strain as a function of applied stress for NiTiPd alloys of varying Pd content.

3.3 Monotonic isothermal stress-strain behavior

As a first step in determining the reason for significant plastic deformation at every stress level in these alloys, the strength of the martensite and austenite phases was determined. Monotonic tensile curves at temperatures of M_f-50°C and A_f+50°C for alloys tested in the virgin state (extruded and heat treated at 400°C/1hr) are shown in Figures 9 and 10 and represent the basic tensile properties of the martensite and austenite states, respectively.

In the martensite state, all of the alloys except $Ni_{3.5}Ti_{50.5}Pd_{46}$ displayed tensile curves having three distinct segments: an initial non-linear elastic section, a stress plateau or region of low work hardening, followed by a final region of higher work hardening. Despite all of the tests being 50°C below the M_f and at approximately the same normalized temperature (T_{Mf-50}/T_{Mf}) with respect to absolute zero, the plateau region starts at a higher stress and can be seen to increase in slope and decrease in length with increasing Pd content.

The monotonic tensile curves in the austenite range display steep linear elastic behavior and also exhibit a short plateau after yielding. In the lower Pd alloys, the plateau is likely due to a stress induced transformation of martensite which is followed closely by a change in slope and deformation of the austenite. In the alloy with 46 at.% Pd, the elastic-plastic nature of the stress-strain curve is due to dynamic recovery during deformation of the austenite. In the lower Pd alloys, the plateau in the austenite is very short compared to that in the martensite, suggesting that very little austenite is being transformed to martensite, and thus the yielding behavior is very close to that of pure austenite, where deformation occurs by dislocation processes.

Yield stresses were determined by the 0.2% offset method and are shown as a function of Pd content in Figure 11. Yielding in the martensite phase is due to the onset of twin boundary motion or detwinning, while yielding of the austenite phase is shown as being due to the onset of typical dislocation processes or slip. It can be seen that the critical stress for twin boundary movement or reorientation increases with increasing Pd content from 97 to 365 MPa, while the critical stress for slip decreases with increasing Pd content from 437 to 98 MPa.

A minimum condition for good work output, or strain recovery under load, in a shape memory alloy is that the material must have a higher yield stress in the austenite phase than in the martensite phase [29]. This explains the very poor performance of the $Ni_{3.5}Ti_{50.5}Pd_{46}$ alloy and its inability to produce any meaningful work output. However, this does not explain the poor dimensional stability or significant permanent deformation observed in the alloys with lower Pd content. Ideally, when shape memory alloys are thermally cycled under a constant stress one would expect strain by detwinning of the martensite, which will be fully recovered as the material is thermally cycled into the austenite state, leaving only an elastically strained austenite. But, in reality, not all of the strain is recovered during the thermal cycling of any of the NiTiPd alloys, resulting in permanent deformation (Figure 8), even when the austenite phase is considerably stronger than the martensite (Figure 11). Therefore, additional factors critical to the performance of these high-temperature shape memory alloy must be involved.

3.4 Shape memory behavior and plastic deformation of the martensite

As mentioned previously, very little is actually known about the deformation mechanisms operating along the stress-strain curve in shape memory alloys, particularly in the high-temperature ternary systems, where the behavior may differ significantly from that of binary alloys. In this study, an unconstrained strain recovery "step test" was used to determine the approximate stress along the monotonic tensile stress-strain curve where slip processes begin to operate, following the procedures described in Figure 2. In Figure 12, the loading, residual strain, and permanent strain curves from the step test performed on the $Ni_{19.5}Ti_{50.5}Pd_{30}$ alloy are shown. The residual strain is the amount of strain remaining in the sample after loading to a particular strain and then unloading back to zero stress at a constant temperature. The permanent strain is the amount of this residual strain remaining after the sample is then thermally cycled at zero stress through the transformation and back to the test temperature. If all the residual strain is recovered during heating then there will be no permanent or plastic strain left in the sample. The residual strain and permanent strain as a function of the maximum stress reached in each cycle of the step test is shown superimposed in Figure 12. To correctly use and understand this plot, it is necessary to refer to the various curves on an equal stress basis. As an example, for the loading curve where a maximum stress of 400 MPa was reached, the maximum applied strain was 3.2%, the residual strain after unloading was 2.4%, and the permanent strain after thermal cycling was 0.87%. Using Equation 1, we can calculate the fraction of strain recovered to be 63%.
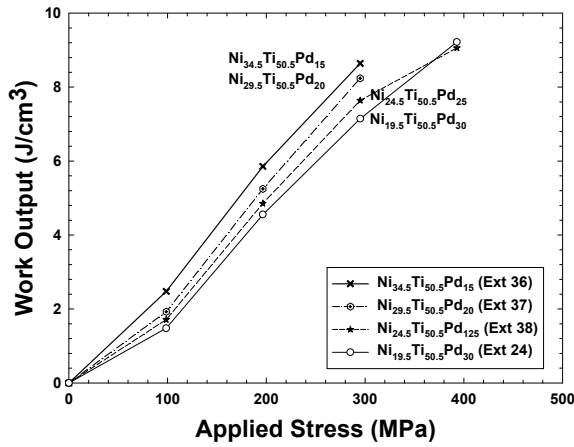
Figure 7: Work output as a function of applied stress for NiTiPd alloys of varying Pd content.
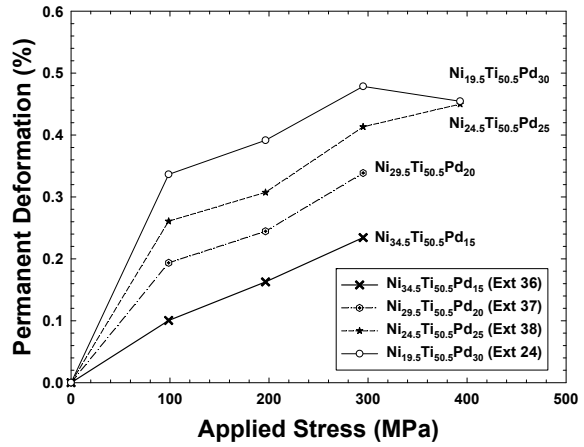

Figure 8: Permanent deformation during thermal cycling at different stress levels for NiTiPd alloys of varying Pd content.
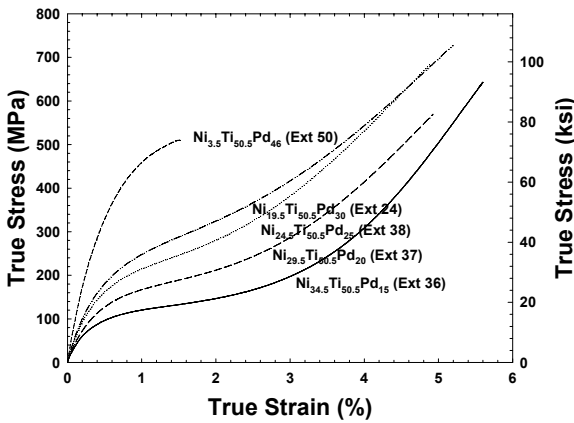

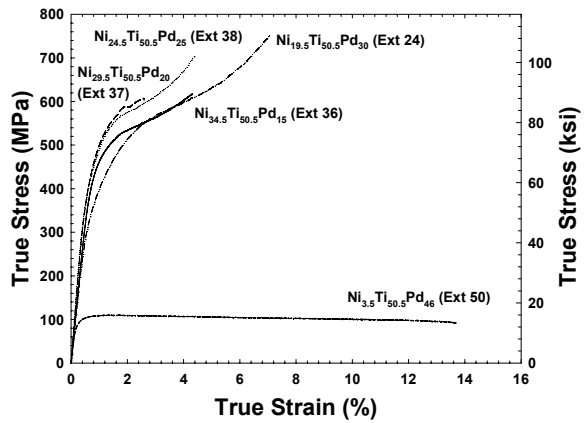**Figure 9:** Monotonic tensile behavior of the alloys in the martensite state – test temperature of M_f-50°C.

Figure 10: Monotonic tensile behavior of the alloys in the austenite state – test temperature of A_f+50°C.
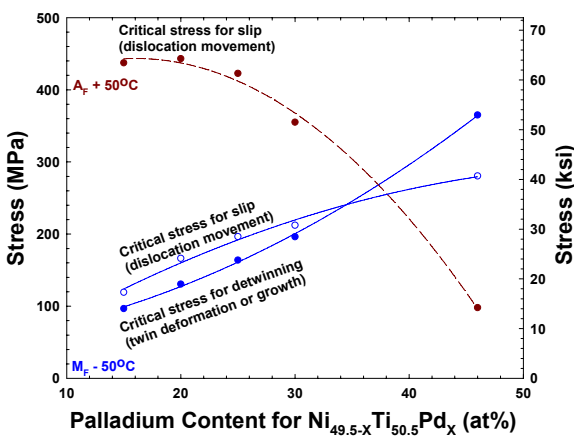

Figure 11: Critical stress data for NiTiPd alloys determined from monotonic tensile tests and strain recovery behavior.

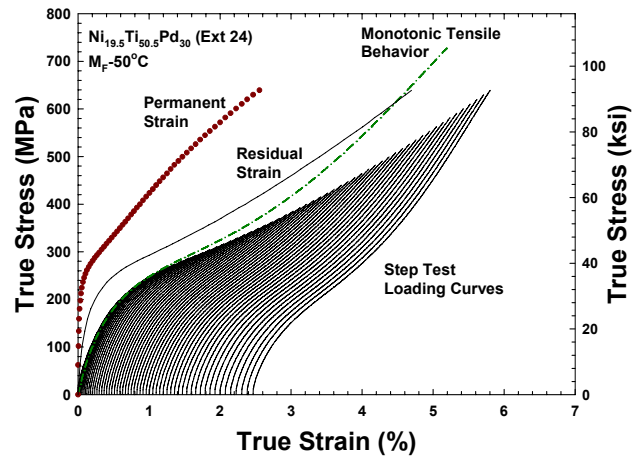**Figure 12:** Incremental stress-strain loading curves and resulting residual strain and permanent strain as a function of stress for $Ni_{19.5}Ti_{50.5}Pd_{30}$.

Figure 13 shows for all five alloys the fraction of the residual strain that was recovered by heating the sample into the austenite state and then cooling it back to the test temperature. Because only two of the alloys ever attained 100% recovery of the residual strain (meaning that all the residual strain was thermally recovered), the 90% recovery level was arbitrarily chosen as a defining fraction for the alloys. It can be seen that for the $Ni_{34.5}Ti_{50.5}Pd_{15}$ alloy, 90% or more strain was recovered when the alloy was strained to a maximum of 2.2% strain. For the alloys with 20, 25, and 30 at.% Pd, the maximum strain the alloy could experience with 90% recovery or more was 1.5, 1, and 0.4%, respectively. The $Ni_{3.5}Ti_{50.5}Pd_{46}$ alloy never got above 45% recovery at any strain level, due to extensive non-recoverable slip that occurred prior to inducing any recoverable deformation by twinning during the straining process.

While the recovery fractions may appear low compared to the results of other authors [30, 31], it must be noted again that the materials were in the as-extruded, or "virgin", state, which means that they had not been strengthened by any method. Our materials would be more closely related to the arc melted, homogenized, and hot rolled baseline $Ni_{20}Ti_{50}Pd_{30}$ alloy tested at 200°C by Shimizu et al. [31]. Comparing the data from Shimizu's alloy to the $Ni_{19.5}Ti_{50.5}Pd_{30}$ alloy tested here, one can see that the data is fairly comparable up to a maximum applied strain of 2%. The differences after this may be due to material properties, calculation method (Shimizu et al. use the strain at A_f+100°C as the permanent strain), or the difference in step size (0.1% for this study and 0.5 to 1% by Shimizu et al.) The additional steps needed to achieve the same strain levels may have led to the diminished recovery as the samples were cycled a larger number of times into the high temperature austenite state.

Figure 14 is a plot of the permanent or plastic strain versus maximum applied strain for all five alloys. In the alloys containing lower levels of Pd, the permanent strain at a specific maximum applied strain is much lower than that of the alloys with high Pd contents. This means that those with lower Pd contents, such as $Ni_{34.5}Ti_{50.5}Pd_{15}$, exhibit a higher ratio of recoverable twin boundary motion or reorientation to non-recoverable slip deformation at a given strain level than those alloys containing more Pd.

Figure 15 shows the maximum stress versus permanent strain data from the step tests on all five alloys at M_f-50°C. These curves essentially represent the permanent deformation behavior of the martensite with recoverable strain processes factored out. Consistent with previous stress-strain curves, a "yield point" for slip in the martensite of each data set was determined using the 0.02% offset method and plotted along with the yield data from the monotonic tensile curves from Figure 11. Even though this permanent strain may be representative of more than just dislocation motion, i.e. non-recoverable martensite twins [25, 26, 27], the "yield" points from the step tests in Figure 15 are labeled in Figure 11 as being representative of the critical stress for slip in the martensite. It can be seen that while the critical stress for detwinning in the martensite increases with increasing Pd content, the difference between it and the critical stress for slip in the martensite decreases until in the $Ni_{3.5}Ti_{50.5}Pd_{46}$ alloy the critical stress for detwinning is 84 MPa higher than the critical stress for slip. These critical stresses (for detwinning and slip) are superimposed on the monotonic isothermal tensile curves in Figure 16 to make it easier to visualize where detwinning and gross slip processes begin to operate. The detwinning yield stresses all lie approximately at the beginning of the stress plateau. In the alloys with lower Pd content, detwinning operates alone for approximately 1/5th of the distance along the plateau before dislocation slip occurs. After slip begins, slip and detwinning occur simultaneously until all of the mobile martensite twins have been reoriented or pinned in place. In the alloy with 46 at.% Pd, slip occurs well before detwinning can operate.

4.0 DISCUSSION

As a minimum condition, alloys with large relative differences in the critical stress for slip in the austenite and critical stress for detwinning or twin formation in the martensite, $\sigma_y^A > \sigma_y^M$, have the potential to generate significant work during load-biased thermal cycling, while alloys with low or negative relative stresses have no chance of exhibiting properties useful for actuator-type applications. However, this condition is not sufficient to ensure reasonable work output with good dimensional stability. In NiTiPd, the difference between the critical stress for slip and the critical stress for detwinning in the martensite also plays a role in the work output and permanent deformation behavior of shape memory alloys thermally cycled under load.

Figure 17 shows that the work output at 295 MPa decreases slightly with Pd content between 15 and 30 at.% Pd, but at 46 at.% Pd, the work output catastrophically drops to zero. This is consistent with the findings from both the monotonic tensile tests and strain-recovery tests on these alloys. These tests showed that the relative yield stress between σ_y^A and

σ_y^M decreases from 341 MPa in $Ni_{34.5}Ti_{50.5}Pd_{15}$ to 159 MPa in $Ni_{19.5}Ti_{50.5}Pd_{30}$, and then to -267 MPa for the $Ni_{3.5}Ti_{50.5}Pd_{46}$ alloy (Figure 11). Also, the difference between the critical stress for slip and the critical stress for twin motion in the martensite $\sigma_{c\ slip}^M$-σ_y^M decreases overall from 23 to 17 MPa with the increase from 15 to 30 at.% Pd, and at 46 at.% Pd is -84 MPa. At some point between 30 and 46 at.% Pd, probably around 37 at.% Pd, the relative yield stress between the martensite and austenite and the difference in critical stresses for slip and detwinning in the martensite equal zero. At lower Pd contents than this crossover composition, work is possible because an applied stress results predominantly in detwinning before slip occurs, or concurrent with slip processes. At the highest Pd content, any stress high enough to cause detwinning in the martensite also produces slip in the martensite, and subsequently a much greater amount of slip in the austenite when the alloy is cycled through the transformation.

In all of the studied alloys, some amount of permanent deformation occurs at every stress level, even in the alloy with the lowest Pd content, though the amount of permanent deformation increases in an approximately linear fashion with increasing Pd content between 15 and 30 at.% Pd. For example, permanent deformation after thermal cycling under 295 MPa (constant stress) increases from 0.23 at 15 at.% Pd to 0.48% at 30 at.% Pd (Figure 18). This result is consistent with the estimates for the onset of twin boundary movement or detwinning and slip of the martensite performed in this study, which occur at essentially the same stress levels for alloys containing 15 to 30 at.% Pd, especially given the use of an offset method for determination of the critical stresses (so that actual slip processes are operating at some extent at lower stresses). The data is also consistent with the earlier results discussed in Figures 13, 14, and 16, which indicated that a higher percentage of the strain applied to the lower Pd alloys is recoverable, and therefore less of the applied strain ends up as permanent deformation. Therefore, some plastic deformation is unavoidable in all alloys, with improved behavior inversely proportional to the Pd level. In alloys with high Pd content (>~37 at.%), slip occurs well before detwinning; therefore there is little to no recoverable deformation that can occur to produce work, and thus the alloy exhibits large amounts of non-recoverable permanent deformation when thermally cycled under load.

The data in total is also very useful in revealing the critical factors that would lead to the development of superior alloys for actuator-type applications: a low stress for detwinning of the martensite and a high stress for yielding by any type of slip processes in both the austenite and martensite. Thus the key to developing dimensionally stable, high-temperature shape memory alloys with good work output is to prevent the operation of all dislocation-mediated deformation processes while not greatly affecting detwinning.

5.0 SUMMARY AND CONCLUSION

Monotonic isothermal tensile tests and no-load strain recovery step tests were used to explain the behavior of high-temperature NiTiPd shape-memory alloys in actuator-type constant-load thermal cycling tests (load-biased tests). With increasing Pd content, the critical stress for slip in the austenite state decreased while the critical stress for detwinning and the critical stress for slip in the martensite increased, all of which lead to a decrease in work output. While the critical stress for slip in the martensite phase increased with increasing Pd content, the difference between it and the critical stress for detwinning decreased until in the alloy with 46 at.% Pd, slip occurs in the alloy well before any recoverable twinning processes. Therefore, both increasing stress and increasing Pd content result in an increase in permanent deformation strain in the alloys. Also, the fraction of strain that can be recovered in an alloy decreases with increasing Pd content.
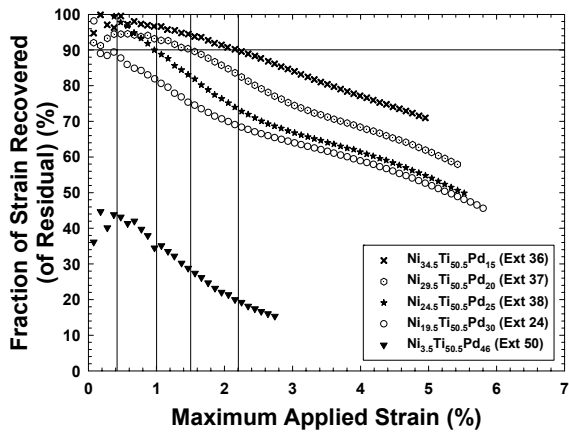

ACKNOWLEDGEMENTS

Figure 13: Fraction of residual strain recovered by thermal cycling the alloys through the transformation to the austenite state and back to the test temperature.
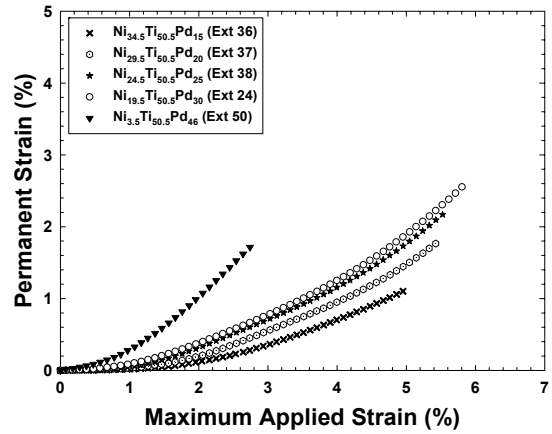

Figure 14: Permanent strain as a function of maximum applied strain for the five alloys studied.
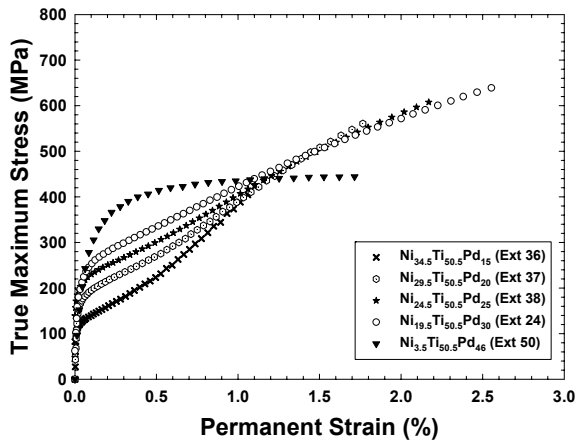

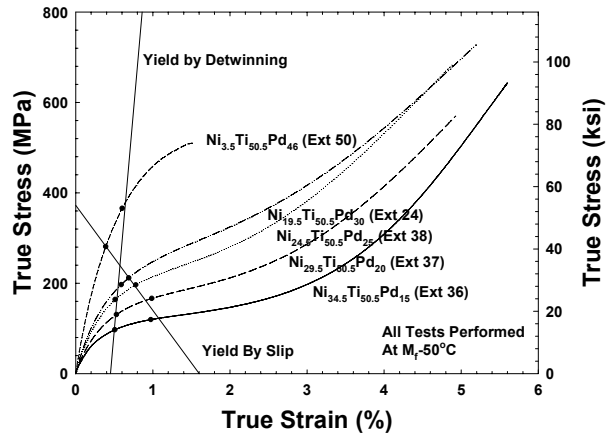**Figure 15**: Permanent strain data from the five alloys.

Figure 16: Yield data determined from the monotonic tensile tests and strain-recovery step tests superimposed on the monotonic tensile curves of the martensite.
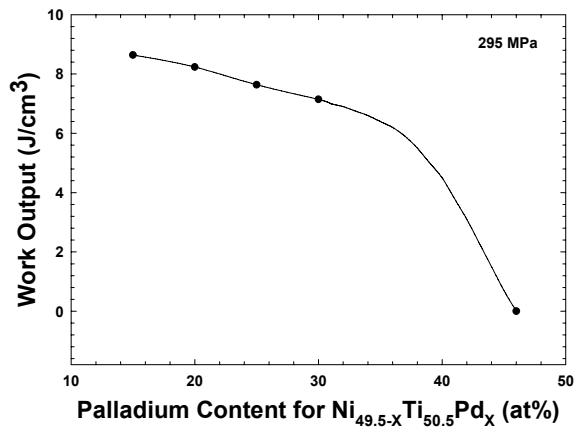

Figure 17: Work output determined from transformation strain in load-biased tests performed at 295 MPa.
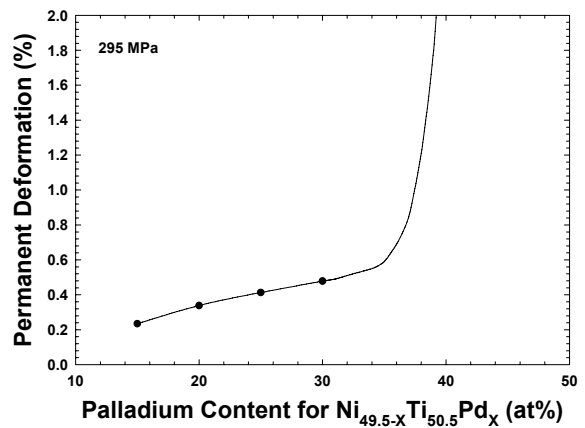

Figure 18: Permanent deformation strain in load-biased tests performed at 295 MPa.

REFERENCES

1. L.C. Chang and T.A. Read, "Plastic deformation and diffusionless phase changes in metals - The gold-cadmium beta phase," *Trans. AIME* 189**,** 47-52 (1951).
2. W.J. Buehler *et al.*, "Effect of low temperature phase changes on the mechanical properties of alloys near composition of TiNi," *J. Appl. Phys.* 34, 1475-1477 (1963).
3. K.N. Melton, "Ni–Ti based shape memory alloys," *Engineering Aspects of Shape Memory Alloys*, T.W. Duerig, K.N. Melton, D. Stöckel, and C.M. Wayman, eds., Butterworth-Heinemann, Ltd., Boston, MA, 1990, 21-35.
4. G. Rondelli *et al.*, "Corrosion properties of NiTi shape-memory alloys," *MRS International Meeting on Advanced Materials Proceedings, vol. 9,* K. Otsuka and K. Shimizu, eds., MRS, Pittsburg, PA, 1989, 237-242.
5. K.D. Skrobanek *et al.,* "Stress-optimized shape memory microactuator," *Proc. of SPIE.* 2779, 499-504 (1996).
6. P. Krulevitch *et al.,* "Thin film shape memory alloy microactuators," *J. Microelectromech. Sys.* 5**,** 270–282 (1996).
7. J.L. Proft and T.W. Duerig, "The mechanical aspects of constrained recovery," *Engineering Aspects of Shape Memory Alloys*, T.W. Duerig, K.N. Melton, D. Stöckel, and C.M. Wayman, eds., Butterworth-Heinemann, Ltd., Boston, MA, 1990, 115-129.
8. K. Otsuka and X Ren, "Physical metallurgy of Ti-Ni-based shape-memory alloys," *Prog. Maters. Sci.* 50, 511-678 (2005).
9. H.C. Donkersloot and J.H. Van Vucht, "Martensitic transformations in gold-titanium, palladium-titanium, and platinum-titanium alloys near the equiatomic composition," *J. Less-Common Mets.* 20, 83-91 (1970).
10. P.G. Lindquist and C.M. Wayman, "Shape memory and transformation behavior of martensitic Ti-Pd-Ni and Ti-Pt-Ni alloys," *Engineering Aspects of Shape Memory Alloys*, T.W. Duerig, K.N. Melton, D. Stöckel, and C.M. Wayman, eds., Butterworth-Heinemann, Ltd., Boston, MA, 1990, 58-68.
11. O. Rios *et al.*, "Characterization of ternary NiTiPt high-temperature shape memory alloys," *Smart Structures and Materials 2005: Active Materials: Behavior and Mechanics*, SPIE Conf. Proc. 5761, 376-387 (2005).
12. S.K. Wu, "Interstitial ordering and martensitic transformation of titanium-nickel-gold alloys," *Ph.D. Dissertation*, University of Illinois, Urbana-Champaign, Illinois, 1986.
13. D.N. AbuJudom *et al.*, "High transformation temperature shape memory alloy," *U.S. Patent No. 5,114,504* (1992).
14. D.R. Angst *et al.*, "The effect of hafnium content on the transformation temperatures of $Ni_{49}Ti_{51-X}Hf_X$ shape-memory alloys," *J. Phys. IV.,* 5, C8-747 - C8-752 (1995).
15. J.H. Mulder *et al.*, "Martensitic transformations and shape memory effects in Ti-Ni-Zr alloys", in *ICOMAT-92: Proceedings of the International Conference on Martensitic Transformations*, Monterey Institute for Advanced Studies, Carmel, California, 1993, 869-874.
16. Z. Pu *et al.*, "Martensite transformation and shape-memory effect of NiTi-Zr high-temperature shape-memory alloys," *Smart Structures and Materials 1995: Smart Materials*, SPIE Proc. 2441, 171-178 (1995).
17. K. Otsuka and C.M. Wayman, *Shape Memory Materials*, Cambridge University Press, Cambridge, England, 1998.
18. K.N. Melton and O. Mercier, "The mechanical properties of NiTi-based shape memory alloys," *Acta Metall.* 29, 393-398 (1981).
19. C.M. Wayman and H.R.P. Inoue, "Crystallographic transformations," in *Intermetallic Compounds*, John Wiley and Sons, New York, 1995.
20. N.G. Boriskina and E.M. Kenina, "Phase equilibria in the Ti-TiPd-TiNi system alloys," in *Titanium 80, Science & Technology, Proceedings of the 4th International Conference on Titanium*, H. Kimura and O. Izumi, eds., The Metallurgical Society of AIME, Warrendale, PA., 1980, 2917-2927,
21. N.M. Matveeva *et al.*, in *Stable and Metastable Phase Equilibrium in Metallic Systems*, M.E. Drits, ed., Nauka, Moscow, 1985, 25.
22. G.F. Bastin and G.D. Rieck, "Diffusion in the titanium-nickel system I: Occurrence and growth of the various intermetallic compounds," *Metall. Trans.* 5, 1817-1826 (1974).
23. M.V. Nevitt, "Stabilization of certain Ti_2Ni-type phases by oxygen," *Trans. Metall. Soc. AIME* 218, 327-331, 1960.
24. M. Nishida *et al.*, "Precipitation processes in near-equiatomic TiNi SMA," *Metall. Trans. A.* 17A, 1505-1515 (1986).
25. S. Miyazaki *et al.*, "Effect of cyclic deformation in the pseudoelasticity characteristics of TiNi alloys," *Metall. Trans. A.* 17A, 115-120 (1986).
26. T.J. Lim and D.L. McDowell, "Degradation of an Ni–Ti alloy during cyclic loading," *Proc. of the 1994 North American Conference on Smart Structures and Materials, SPIE*, 153–165 (1994).

27. D.A. Miller and D.C. Lagoudas, "Influence of cold work and heat treatment on the shape memory effect and plastic strain development of NiTi," *Mater. Sci. and Eng. A.* 308, 161-175 (2001).

28. R. Noebe *et al.*, "Properties of a $Ni_{19.5}Pd_{30}Ti_{50.5}$ high-temperature shape memory alloy in tension and compression," *Smart Structures and Materials 2006: Active Materials: Behavior and Mechanics*, *SPIE Conf. Proc.* 6170, Paper No. 617010 (2006).

29. R. Noebe *et al.*, "Properties and potential of two (Ni,Pt)Ti alloys for use as high-temperature actuator materials," *Smart Structures and Materials 2005: Active Materials: Behavior and Mechanics*, *SPIE Conf. Proc.* 5761, 364-375 (2005).

30. D. Goldberg *et al.*, "Improvement of a $Ti_{50}Pd_{30}Ni_{20}$ high temperature shape memory alloy by thermomechanical treatments," *Scripta Metall. Mater.* 30, 1349-1354 (1994).

31. S. Shimizu *et al.*, "Improvement of shape memory characteristics by precipitation hardening of Ti-Pd-Ni alloys," *Maters. Letters* 24, 23-29 (1998).